Luminescence spectroscopy of matrix-isolated $z\,^6P$ state atomic manganese

Martin A. Collier[a] and John G. McCaffrey[b]
Department of Chemistry, National University of Ireland—Maynooth, Maynooth, County Kildare, Ireland

(Received 8 December 2004; accepted 21 February 2005; published online 9 May 2005)

The relaxation of electronically excited atomic manganese isolated in solid rare gas matrices is observed from recorded emission spectra, to be strongly site specific. $z\,^6P$ state excitation of Mn atoms isolated in the red absorption site in Ar and Kr produces narrow $a\,^4D$ and $a\,^6D$ state emissions while blue-site excitation produces $z\,^6P$ state fluorescence and broadened $a\,^4D$ and $a\,^6D$ emissions. Mn/Xe exhibits only a single thermally stable site whose emission at 620 nm is similar to the broad $a\,^6D$ bands produced with blue-site excitation in Ar and Kr. Thus in Ar(Kr), excitation of the red site at 393 (400) nm produces narrow line emissions at 427.5 (427.8) and 590 (585.7) nm. From their spectral positions, linewidths, and long decay times, these emission bands are assigned to the $a\,^4D_{7/2}$ and $a\,^6D_{9/2}$ states, respectively. Excitation of the blue site at 380 (385.5) nm produces broad emission at 413 (416) nm which, because of its nanosecond radiative lifetime, is assigned to resonance $z\,^6P \rightarrow a\,^6S$ fluorescence. Emission bands at 438 (440) and 625 (626.8) nm, also produced with blue-site excitation, are broader than their red-site equivalents at 427.5 and 590 nm (427.8 and 585.7 nm in Kr) but from their millisecond and microsecond decay times are assigned to the $a\,^4D$ and $a\,^6D$ states. The line features observed in high resolution scans of the red-site emission at 427.5 and 427.8 nm in Mn/Ar and Mn/Kr, respectively, have been analyzed with the W_p optical line shape function and identified as resolved phonon structure originating from very weak ($S=0.4$) electron-phonon coupling. The presence of considerable hot-phonon emission (even in 12 K spectra) and the existence of crystal field splittings of 35 and 45 cm^{-1} on the excited $a\,^4D_{7/2}$ level in Ar and Kr matrices have been identified in W_p line shape fits. The measured matrix lifetimes for the narrow red-site $a\,^6D$ state emissions (0.29 and 0.65 ms) in Ar and Kr are much shorter than the calculated (3 s) gas phase value. With the lifetime of the metastable $a\,^6D_{9/2}$ state shortened by four orders of magnitude in the solid rare gases, it is clear that the probability of the "forbidden" $a\,^6D \rightarrow a\,^6S$ atomic transition is greatly enhanced in the solid state. A novel feature identified in the present work is the large width and shifted ^4D and ^6D emissions produced for Mn atoms isolated in the blue sites of Ar and Kr. In contrast, these states produce narrow, unshifted (gas-phase-like) ^4D and ^6D state emissions from the red site. © *2005 American Institute of Physics*.
[DOI: 10.1063/1.1889426]

I. INTRODUCTION

Although the absorption[1] and magnetic circular dichroism (MCD)[2] spectroscopies of matrix-isolated atomic manganese have been studied in detail, no reports of the luminescence of Mn/RG solids have appeared in the literature. Indeed systematic studies of the luminescence[3] of matrix-isolated transition metal atoms have not yet been presented. However, a few studies have appeared such as those by Nixon and co-workers[4] on Fe, Co, and Ni atoms and that of Pellin *et al.*[5] on atomic Cr and Mo. The coinage metals have been studied by the groups of Kolb[6] and Ozin.[7] These studies have shown that the emission linewidths depend very strongly on the electronic configurations involved in the transitions. Thus, $d \rightarrow s$ transitions are observed to be narrow and unshifted from their gas phase positions, while $p \rightarrow s$ transitions are now well known to be broad, exhibiting large Stokes-shifted emission. More recently, our group at Maynooth has looked at the luminescence of matrix-isolated atomic Zn,[8] Cd,[9] and Hg[10] and observed that the emission is dominated by $P \rightarrow S$ transitions. To date, no work has appeared on the luminescence of atomic Mn whose absorption[11] is also dominated by $P \leftarrow S$ transitions. However, one study by Moskovits and co-workers[12] on the laser-induced fluorescence of manganese isolated in Kr matrices, attributed featureless bands in the red spectral region to Mn_2. The present and subsequent contributions[13] reveal the carrier of the emission in this spectral region is actually metastable ^6D state atomic manganese. As will be shown in the present study,[14] the reasons for this earlier misassignment arise from the novel behavior of atomic manganese when excited in the "blue" site of isolation of broad, large Stokes-shifted $d \rightarrow s$ emission. Excitation of Mn atoms isolated in the "red" sites produces the expected narrow $d \rightarrow s$ line emissions, unshifted from the gas phase position.

The work of closest relevance to the present is that of Pellin *et al.*[5] on atomic Cr. Like Mn, atomic Cr exhibits an S ground state and the resulting absorption spectra are domi-

[a]Present address: Laboratoire Francis Perrin, CEA Saclay, France.
[b]Electronic mail: john.mccaffrey@nuim.ie

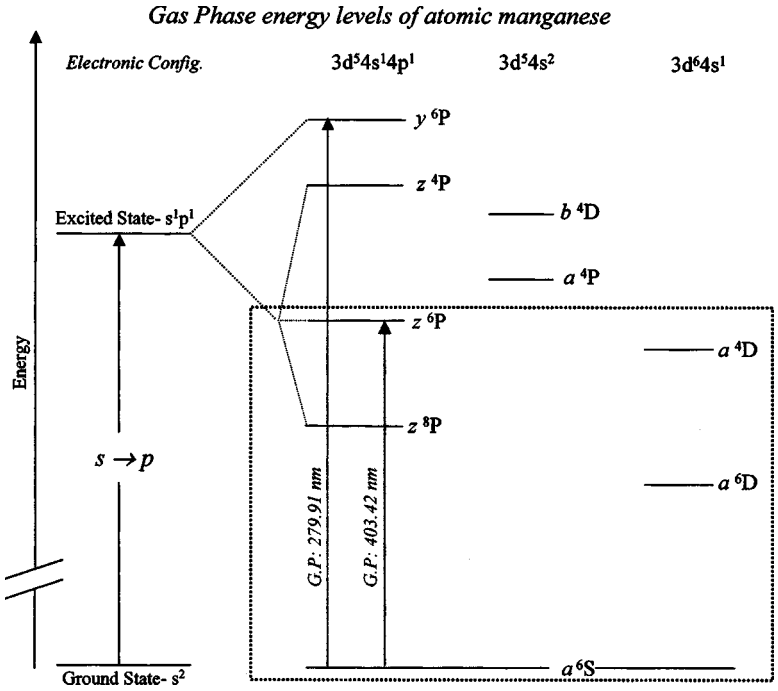

FIG. 1. Schematic representation of the energy levels of gas phase atomic manganese. The fully allowed $y\,^6P_{5/2} \leftarrow a\,^6S_{5/2}$ and $z\,^6P_{5/2} \leftarrow a\,^6S_{5/2}$ transitions occurring at 35 726 cm^{-1} (279.91 nm) and 24 788 cm^{-1} (403.42 nm), respectively, are indicated by arrows. The area of the diagram shown in the dotted box, highlights the low-lying excited states that exist below the $z\,^6P$ state and which are accessible in relaxation occurring after $z\,^6P \leftarrow a\,^6S$ photoexcitation utilized in the present study.

nated by $P \leftarrow S$ state transitions. Cr also has many low-lying states derived from *d*-type orbital configurations. However, in Cr the lowest energy excited states are only a few thousand wave numbers above the ground state, so that emission in the visible spectral region is dominated by interexcited state transitions. The equivalent ^6D excited state in Mn is $\approx$17 000 cm^{-1} above the ground state, so that emission from this metastable state to the ground state is then expected in the red spectral region.

In a previous contribution[15] bands present at 385.5 nm (25 940 cm^{-1}) and 401.9 nm (24 881 cm^{-1}) in the absorption spectrum of manganese isolated in Kr were both assigned to the $z\,^6P \leftarrow a\,^6S$ transition of manganese atoms. Mn/Kr was the only member of the Mn/RG matrix systems where absorption spectra lead to the identification of two distinct sites of atomic isolation. On the basis of their relative spectral positions and abundances, the sites identified were labeled blue (1°) at 385.5 nm and red (2°) at 401.9 nm. It should be noted that the site labels used in Kr are not interchangeable with those used for Mn/Ar, where 1° and 2° refer to the red and blue sites, respectively. The absorption spectra of Mn/Xe samples exhibited only a single thermally stable site of atomic isolation. A polarizability analysis of the matrix shifts exhibited by these sites in the three rare gases Ar, Kr, and Xe, allowed the association of the single site in Xe with the blue sites in Ar and Kr. This analysis led to the identification of single vacancy site occupancy for the blue-site bands and tetravacancy site occupancy for the red features.

In the present contribution the emission spectroscopy of atomic Mn isolated in solid rare gas matrices, resulting from photoexcitation of the lowest energy resonance, viz the $[\mathrm{Ar}]3d^5 4s4p\ z\,^6P \leftarrow a\,^6S [\mathrm{Ar}]3d^5 4s^2$ transition, is presented. Analysis of the luminescence of atomic Mn isolated in RG solids is challenging for a number of reasons. (i) Atomic Mn possesses[16] the excited $[\mathrm{Ar}]3d^6 4s^1$ and $[\mathrm{Ar}]3d^5 4s^2$ electronic configurations in addition to the $[\mathrm{Ar}]3d^5 4s4p$ configuration accessed in absorption. The last configuration gives rise to two states—the $y\,^6P$ and the $z\,^6P$—that are accessible in fully allowed electric-dipole transitions from the ^6S ground state. To minimize spectral congestion, only the luminescence produced with excitation of the lower energy $z\,^6P$ state is presented in this work. Even for the $z\,^6P$ state, there are three lower energy excited states, thereby providing multiple relaxation channels (both radiative and nonradiative) for excited state populations. The excited states of atomic manganese energetically accessible with $z\,^6P$ excitation are shown in Fig. 1 by the region indicated in the dotted box. (ii) The existence of multiple trapping sites of atomic isolation presents several different "types" of Mn atoms, each capable of exhibiting distinct excited state behaviour, due to the specific guest-host interactions within their matrix cages.

This paper is structured as follows. First, steady-state emission spectra recorded with continuous lamp excitation of the absorption features assigned to the $z\,^6P \leftarrow a\,^6S$ transition of atomic Mn isolated in the rare gases Ar, Kr, and Xe are presented. Excitation spectra recorded by monitoring the resulting emission features are then presented which allow site identification. With this information, high-resolution emission spectra, produced with cw lamp and pulsed laser excitation, allow characterization of the observed emission line shapes for Mn atoms isolated in specific sites. Excited state lifetime measurements made with pulsed laser excitation and line shape simulations generated with the optical W_p function[17] are used to assign the recorded emission bands to transitions of atomic manganese. Temperature-dependent, site-specific emission spectra and lifetime measurements are recorded to provide insight into the nonradiative excited state dynamics leading to the observed atomic emission. Where possible the radiative decay characteristics of the excited states are identified and presented. A summary and compari-

son of the luminescence resulting from Mn $z\,^6P \leftarrow a\,^6S$ excitation in Ar, Kr, and Xe matrices is then made.

II. EXPERIMENT

The vacuum apparatus and the gas handling system used in the preparation of Mn/RG matrix samples has been described in previous publications[18] from our group. Mn vapor was generated by electron bombardment of Mn chunks held in a Mo crucible as outlined in recently presented work[15] on the absorption and excitation spectroscopies of matrix-isolated manganese. All the spectra shown in the present contribution were recorded for samples prepared under low metal loading conditions which, even in Mn/Ar, contain predominately isolated Mn atoms. Emission from Mn/RG samples was recorded[19] with an Acton Research (ARC) 0.5 m SP500i monochromator fitted with three gratings, a 1200 g/mm and a 150 g/mm, both blazed at 300 nm and a 600 g/mm grating blazed at 500 nm. A Hamamatsu *R*928-P photomultiplier tube (PMT), maintained at −20 °C in a Products for Research (Photocool, S600) cooled housing, was used in photon counting mode for detection.

The excitation sources used were either a cw tungsten lamp, dispersed with a 0.3 m ARC SP300i monochromator, or a Nd:YAG (YAG—yttrium aluminum garnet) (Quantel, YG 980E-10) laser normally operating at a repetition rate of 10 Hz. The wavelengths required for manganese atom $z\,^6P$ state excitation in the 360–420 nm spectral region were produced by mixing the 1064 nm YAG fundamental with the dye laser (Quantel, TDL-90) output. For excitation of the blue sites, Rhodamine 590 was the dye material used, while DCM was used for the red-site excitation. A potassium dihydrogen phosphate crystal (Quantel MCC1) was used for frequency mixing while a quartz crystal (Quantel QCC1) was used to compensate for the walk of the resultant beams. Wavelength separation of the UV beam from the YAG and dye laser beams was achieved with a Pellin–Broca prism. The UV output was trained onto the matrix sample (held at 12 K on a CaF_2 window) without focusing optics. Typical laser fluence of 20 μJ/mm^2, was achieved in the UV beam using only the oscillator and preamplifier stages of the TDL-90.

Time-resolved emission spectra (TRES) were recorded using an Andor Technologies iStar DH720 iCCD (intensified charge coupled device) detector mounted on the SP500i imaging spectrograph. A swing mirror in the SP500i allowed the dispersed emitted radiation either to fall directly on the iCCD camera or be diverted at right angles to the photon counting PMT. A personal computer equipped with the Andor iStar software and interface card (CCI–010), allowed control of the iCCD unit and the SP500i monochromator via an RS232 connection. Nanosecond lifetime measurements were made by analyzing the TRES recorded with the iCCD camera. Decay curves at specific emission wavelengths were extracted from the TRES with the Andor software, and the decay times were obtained by fitting single or multiple exponential functions to the extracted curves by a nonlinear least squares method. The decay functions were convoluted with the temporal profile of the YG 980 excitation laser [FWHM (FWHM—full-width at half-maximum) 6 ns] to generate the emission decay profiles. The temporal resolution of TRES recorded with the iCCD camera is ≈6 ns.

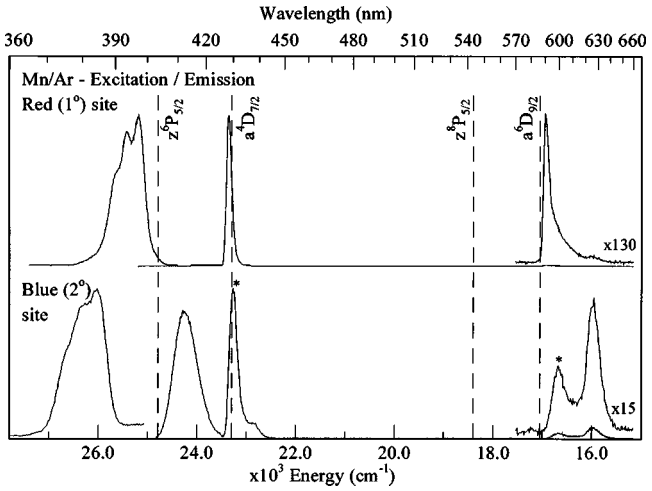

FIG. 2. A summary of the emission spectra recorded at 12 K for a Mn/Ar matrix annealed to 28 K. The excitation spectra were recorded by monitoring emission at 428/590 (top) and 413/625 nm (bottom) for the 1° and 2° sites, respectively. The spectral positions of the gas phase transitions of atomic Mn are shown by the dashed vertical lines. The asterisks indicate emission bands produced with excitation of the thermally unstable 3° site that overlaps both the 1° and 2° sites.

Longer (μs and ms) decay times were recorded with the time-correlated, single photon counting (TCSPC) technique and measured with the photon counting[20] PMT using a 2 GHz multichannel scaler (MCS) (Fast ComTec, Model 7886) as described elsewhere.[19] Start pulses for the iCCD camera and the MCS unit were obtained from the Q-switch prepulse of the YAG laser. The temporal resolution of the photon counting/MCS arrangement has been determined to be ≈500 ns limited largely by the poor pulse-pair resolution of the R928-P PMT when high intensity, low repetition laser is used as the excitation source. This combination of pulsed laser for excitation and photon counting for detection, however, allows the recording of long-lived emission with high sensitivity, as will be demonstrated in the scans done at high spectral resolution on forbidden transitions.

III. RESULTS

All the excitation and emission spectra reported in this study were recorded in the most dilute Mn/RG samples. As shown in our previous absorption work,[15] these samples contain predominately isolated atomic manganese. Because of the extent of the site-and state-specific emissions observed in the Mn/RG matrix systems, only spectra recorded in annealed samples are presented in the present contribution.

A. Excitation and emission of annealed Ar and Kr samples

Figure 2 presents a summary of the emission spectra recorded with red-(1°) and blue-(2°) site excitation at 393.4 and 380 nm, respectively, of a Mn/Ar sample annealed to 30 K. From an inspection of the spectra shown in Fig. 2, it is quite evident that the bands produced are very different,

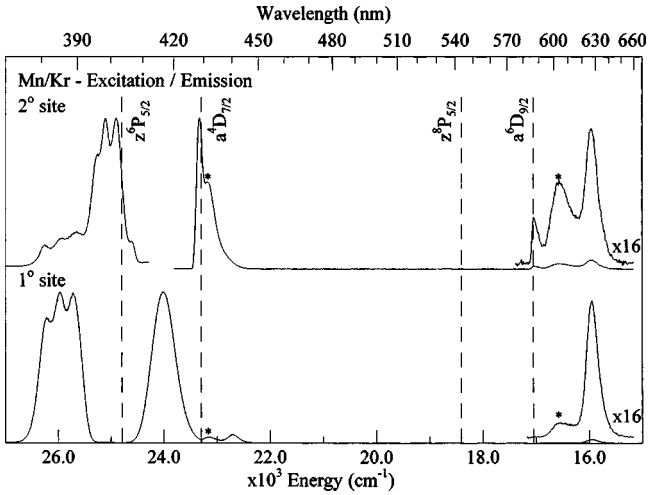

FIG. 3. Emission spectra recorded at 12 K for the Mn/Kr system with site-selective lamp excitation of the Mn $z\,^6P \leftarrow a\,^6S$ transition. The spectra were recorded for Mn/Kr samples deposited at 12 K but annealed to 32 K. The excitation spectra shown on the left were recorded by monitoring emission at 428.4 (top) and 416/626 nm (bottom) for the 2° and 1° sites, respectively. The asterisks indicate the emission bands produced with excitation of the thermally unstable 3° site, remnants of which remain after annealing.

leading to the conclusion that Mn atom emission in Ar is strongly dependent on site occupancy. Thus, excitation of the red site at 393.4 nm gives rise to the structured and narrow emission centered at 427.5 nm and the weak, asymmetric 590 nm band.[21] Blue-site excitation at 380 nm produces three broad emission bands located at 413, 438, and 625 nm. The additional features at 431 and 601 nm have been identified in annealing studies[14] as emission from the thermally unstable (3°) site of Mn atom isolation in Ar.

Figure 3 presents the emission spectra recorded for an annealed Mn/Kr sample with tungsten lamp excitation of the blue-(1°) and red-(2°) site absorptions. The resolved blue (1°) site centered at 385 nm in excitation—the major contribution to the observed absorption band—leads to the emission features centered at 416, 440, and 626.8 nm. The red (2°) site centered at 398 nm produces emission bands at 427.8 and 585.8 nm. The emission features indicated by the asterisks (at 432.4 and 603.8 nm) are due to the 3° site, whose absorption overlaps those of the 1° and 2° sites, and the remnants of which persist after sample annealing. It was found that the intensity of asymmetric emission band at 585.8 nm is enhanced by the annealing procedure for red-(2°) site excitation.

It should be pointed out that the Mn/Kr emission recorded in the 570–650 nm region, shown on the upper right in Fig. 3, bears a very strong resemblance to that reported by Moskovits and co-workers[12] with fixed frequency dye laser excitation at 17 300, 17 350, 17 400, and 17 450 cm^{-1} (578, 576, 575, and 573 nm) of Mn/Kr samples. Thus, the three emission bands at 585.8, 603.8, and 626.8 nm evident in Fig. 3 are also present in Fig. 9 of Ref. 12, but were assigned in the earlier work to transitions of Mn_2. As will be shown ahead, these are the emission bands of metastable $a\,^6D$ state atomic Mn isolated in the three sites present in Kr matrices. Excitation spectra recorded by our group with tuneable dye laser excitation, to appear in a forthcoming publication,[13] prove that the wavelengths used in the earlier laser study[12] pump the forbidden $a\,^6D \leftarrow a\,^6S$ atomic transition, directly populating the metastable ^6D state responsible for the observed red emissions.

TABLE I. Photophysical characteristics of the 1°, 2°, and 3° sites of Mn atom isolation in solid Ar and Kr matrices obtained from the excitation spectra recorded for the $3d^5 4s4p\ z\,^6P \leftrightarrow 3d^5 4s^2\ a\,^6S$ transition. Shown also is the data extracted for the single thermally stable site in Xe. The spectral positions λ, and average full width at half maxima Δ of the three components were identified in Gaussian line shape analyses of the threefold split excitation bands. Matrix to gas phase frequency shifts δ for the atomic Mn $z\,^6P_{5/2} \leftarrow a\,^6S_{5/2}$ transition (G.P.: 24 788.05 cm^{-1}) are presented in wave number units. The frequency shifts were calculated with respect to the central feature of the observed threefold pattern.

Site	Components	λ(nm)	$E(cm^{-1})$	$\Delta(cm^{-1})$	$\delta(cm^{-1})$
		Mn/Ar			
	1	389.9	25 644		
1°	2	393.4	25 421	253	+633
	3	397.2	25 174		
	1	375.5	26 632		
2°	2	380.0	26 319	392	+1531
	3	384.7	25 992		
	1	380.1	26 309		
3°	2	389.9	25 647	710	+859
	3	398.1	25 121		
		Mn/Kr			
	1	381.4	26 219		
1°	2	385.0	25 974	295	+1187
	3	388.8	25 720		
	1	395.9	25 259		
2°	2	398.3	25 107	203	+319
	3	401.6	24 900		
	1	387.6	25 800		
3°	2	393.7	25 400	484	+612
	3	401.6	24 900		
		Mn/Xe			
	1	392.2	25 497		
1°	2	395.5	25 284	270	+496
	3	399.2	25 050		

The strong similarity between the red-site emissions in Ar and Kr matrices is evident by comparing the upper panels in Figs. 2 and 3. The lower traces in these figures reveal the strong similarity between the blue sites in these two solids. Photophysical parameters extracted from the excitation bands recorded for three sites present in Ar and Kr matrices are collected in Table I.

B. Mn/Kr and Mn/Ar

In this section, the spectral and temporal characteristics of each of the observed emission bands in the Mn/Kr system are examined in detail. For reasons of space limitation, only a summary of the results obtained in the analysis of the closely corresponding emission bands in the Mn/Ar system will be presented. In the sections that follow, the Ar data are presented in parentheses. Complete annealing and site details of Mn/RG matrices are to be found in Ref. 14.

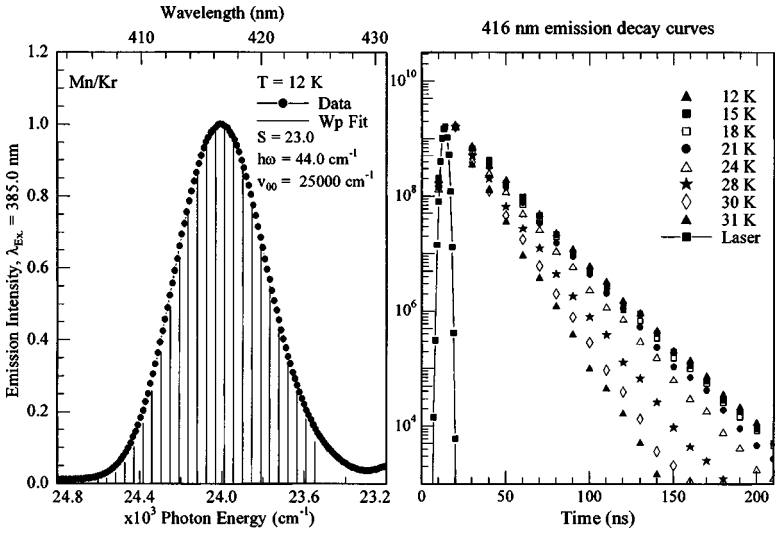

FIG. 4. An emission spectrum and its W_p line shape fit recorded at 12 K for the 416 nm band produced with pulsed laser excitation at 385 nm. Decay profiles of the 416 nm emission feature were extracted from time-resolved emission spectra recorded at the specified temperatures. The temporal profile of the laser excitation source at 385 nm is also shown.

1. Blue site: 416 nm Kr (413 nm Ar) emission

The dominant emission feature produced in Mn/Kr with blue-site $z\,^6P$ excitation at 385 nm occurs at 416 nm exhibiting, as shown on the left in Fig. 4, a linewidth of 505 cm^{-1}. A W_p line shape fit of the emission band with Eq. (1) of Ref. 19 is also shown on the left. A description of the procedure followed in the W_p fits is given ahead in Sec. III B 4 and in Ref. 19. Due to the lack of resolved phonon structure on this emission band, the most probable high frequency mode in the phonon spectrum[22] of solid Kr is used for the fit conducted. As a result of the range of phonon frequencies that exist, the fit shown is not definitive. However, the large electron-phonon coupling strength ($S=23$), and the associated broadband profile are indicative of a $P\rightarrow S$ type electronic transition.

In an attempt to state assign the 416 nm emission band, its temporal decay was recorded and analyzed. On the right-hand side of Fig. 4 the recorded emission decay is shown on a semilog plot, clearly indicating that the decay occurs on a nanosecond time scale. Fitting the emission decay profile required the use of a double-exponential function, with decay times of 46.4 and 30.5 ns. From the dominance of the shorter component it is identified as the observed excited state lifetime $\tau_{obs}=30.5$ ns. The temperature dependence of the 416 nm emission decay profile was recorded and is also presented in Fig. 4. This allowed identification of the emission lifetime observed at 12 K(τ_{obs}) as the radiative decay of the excited state τ_{Rad}, because as shown in Fig. 4, the decay profiles were found to be independent of temperature below 18 K.

Application of the effective field correction [Eq. (2), Ref. 19], using 1.428 as the refractive index of solid Kr,[23] leads to a corrected decay time of 55.3 ns. The gas phase lifetime for the fluorescent $z\,^6P\rightarrow a\,^6S$ transition is reported[24] as 58.8 ± 1.4 ns. As the corrected matrix lifetime $\tau_{Cor.}$ is only slightly shorter than the reported gas phase value, the 416 nm emission feature is thereby assigned to resonance $z\,^6P$ state fluorescence. The matrix emission band is therefore redshifted from the gas phase position of the $z\,^6P_{3/2}\leftrightarrow a\,^6S_{5/2}$ transition at 403.56 nm (24 779 cm^{-1}) by 740 cm^{-1}. Its equivalent in solid Ar is located at 413 nm and from the 57.5 ns decay time listed in Table II, this band is also assigned to resonance $z\,^6P$ state fluorescence.

2. Blue site: 440 nm Kr (438 nm Ar) emission

As well as the 416 nm band, blue-site excitation in Mn/Kr produces, as shown in Fig. 3, emission at 440 nm. Although this emission band is weak at 12 K with $z\,^6P$ excitation, its intensity increases with temperature relative to the 416 nm band. Moreover, with blue-site $y\,^6P$ excitation, the 440 nm band dominates emission in the 405–450 nm region. With a linewidth of $\approx$280 cm^{-1}, the moderately broad 440 nm band looks like a $P\rightarrow S$ type transition. However, the W_p line shape fit shown on the left in Fig. 5 reveals a much smaller S value (6) than the value of 23 found on the 416 nm band, assigned to resonance $z\,^6P$ fluorescence in the preceding section.

On the right-hand side of Fig. 5, the temporal decay of the 440 nm emission is shown for an annealed Mn/Kr sample. This plot reveals that the decay time (0.4 s) is extremely long compared with the nanosecond 416 nm fluorescence. The decay profile was acquired, as outlined in the Experiment section, with a multichannel scaler monitoring emission with photon counting detection. Least squares analysis of the decay profile required three exponential functions to achieve an adequate fit and extract the emission decay times. It is apparent from the complicated decay profiles containing, as shown in the inset, a rise time portion, that the 440 nm emission band exhibits complex excited state kinetics. The three decay times extracted at 12 K, range from the shortest component $\tau_3=2.4$ ms (identified as the rise time) to the longest decay time $\tau_1=100$ ms, the dominant component. Decay profiles recorded at temperatures in excess of 12 K are also presented in Fig. 5. It is clear from the pronounced changes exhibited that the excited state decay curves are extremely sensitive to temperature. Of particular note is the removal of the rise time component at temperatures greater that 25 K, shown inset in Fig. 5. A double-exponential fit of the decay profile recorded at 32 K showed two millisecond components. The strong temperature dependence and the

TABLE II. Photophysical characteristics and excited state assignments of the emission features produced with excitation of the $3d^5 4s4p\ z\ ^6P \leftarrow 3d^5 4s^2\ a\ ^6S$ transition of atomic manganese isolated in the two thermally stable sites in Kr and the single site in Xe. λ indicates the emission band center in nanometer units. The full-width at half-maximum intensity of the emission features is denoted by Δ and the matrix shift by δ—both in wave number (cm^{-1}) units. The excited state lifetimes τ are presented with the subscripts Rad. and Cor. to indicate the radiative lifetime of the excited state and the lifetimes corrected for the effective field of the solid state. τ_{obs} indicates the lifetime of the dominant decay component at 12 K. The question marks indicate state assignments that are only tentative.

State	$\nu(cm^{-1})$	Band λ(nm)	$\Delta(cm^{-1})$	$\delta(cm^{-1})$	τ
		Mn gas phase			
$z\ ^6P_{7/2}$	24 809	403.075	⋯	⋯	58.8 ns
$a\ ^4D_{7/2}$	23 297	429.25	⋯	⋯	3000 s
$z\ ^8P_{3/2}$	18 402	543.42	⋯	⋯	101 μs
$a\ ^6D_{9/2}$	17 052	586.43	⋯	⋯	3 s
		Mn/Ar red (1°) site			
$a\ ^4D_{7/2}$	23 392	427.5	7.0	+92	25.3 ms
$a\ ^6D_{9/2}$(?)	16 949	590.0	100	−103	654 μs
		Mn/Ar blue (2°) site			
$z\ ^6P$	24 213	413.0	465	−566	τ_{Cor}=57.5 ns
$a\ ^4D_{7/2}$(?)	22 831	438.0	230	−466	τ>0.1 s
					τ_1=662 μs
$a\ ^6D_{9/2}$(?)	16 000	625.0	260	−1052	τ_2=165 μs
					τ_3=36 μs
		Mn/Kr red (2°) site			
$a\ ^4D_{7/2}$	23 375	427.8	5.4	+78	23.9 ms
$a\ ^6D_{9/2}$(?)	17 085	585.7	65	−18	287 μs
		Mn/Kr blue (1°) site			
$z\ ^6P$	24 038	416.0	505	−740	τ_{Cor}=55.3 ns
$a\ ^4D_{7/2}$(?)	22 727	440.0	280	−570	τ>0.1 s
$a\ ^6D_{9/2}$(?)	15 954	626.8	260	−1097	τ_1=564 μs
		Mn/Xe			
$a\ ^6D_{9/2}$(?)	16 126	620	240	−926	τ_1=1.83 ms

multiexponential nature of the recorded decay profiles do not allow the radiative lifetime of the 440 nm emission to be identified.

Because of the conflicting spectral and temporal data (broad linewidth/long decay time) recorded, the 440 nm emission in solid Kr cannot be immediately state assigned. However, the assignment of this moderately broad band to $z\ ^6P \rightarrow a\ ^6S$ emission, can be ruled out on the basis of the very long decay times measured. For the energetic reasons illustrated in Fig. 1, the only alternative assignment for the 440 nm emission is the $a\ ^4D$ excited state of atomic manganese. The broad emission line shape and the large matrix shift (570 cm^{-1}) make the $a\ ^4D_{7/2} \rightarrow a\ ^6S_{5/2}$ transition assignment problematic. Similar linewidth and decay time behavior, summarized in Table II, was found in the Mn/Ar 438 nm band, leading to the same $a\ ^4D_{7/2}$ state assignment made for

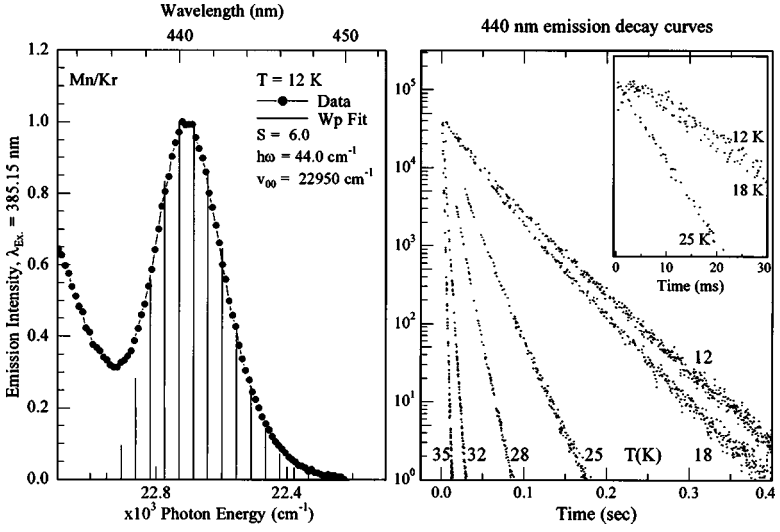

FIG. 5. A W_p line shape fit of the 440 nm emission in Mn/Kr. Decay profiles of the 440 nm emission recorded at the specified temperatures using TCSPC with pulsed laser excitation at 385.15 nm are shown on the right. The behavior of the rise time component at various temperatures is shown inset.

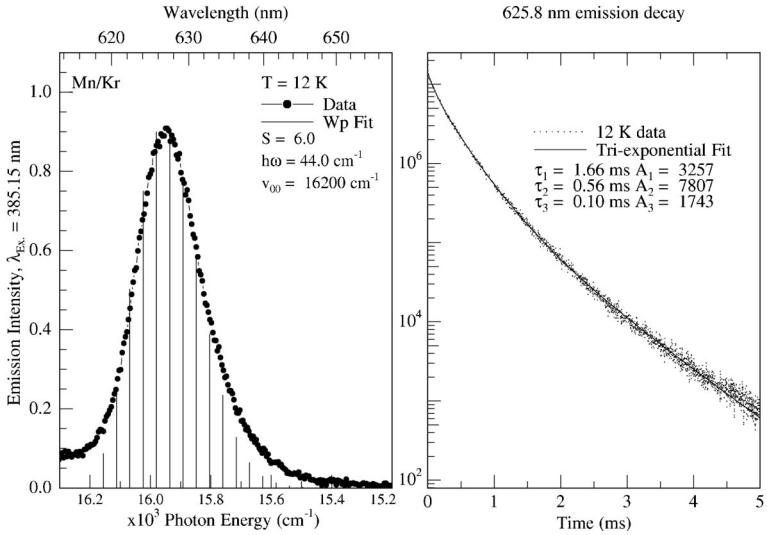

FIG. 6. A W_p line shape fit of the 626 nm emission band in Mn/Kr produced with blue-site excitation at 385.15 nm. A decay profile of the 626 nm emission recorded at 12 K is shown on the right as well as details of a triple-exponential fit.

the blue-site 440 nm emission in Mn/Kr. With these assignments, it is concluded that the $a\,^4D$ state is broadened and shifted considerably in the blue sites of atomic Mn isolation in Ar and Kr matrices.

3. Blue site: 626.8 nm Kr (625 nm Ar) emission

Details of the broad emission band centered at 628.8 nm (15 954 cm^{-1}) resulting from blue-site excitation of the $z\,^6P$ excited state are shown in the left panel of Fig. 6. A W_p line shape fit of this band is also shown. Its S value (6.0), reveals moderate electron-phonon coupling, similar in magnitude to that of the 440 nm band.

An emission decay profile recorded monitoring the 626.8 nm feature at 12 K is shown on the right in Fig. 6. Inspection of the decay profile reveals that complex kinetics leads to the observed emission. A triple-exponential fit allowed the extraction of the decay components 1.67 ms, 564, and 101 μs. The dominant 564 μs decay component is assigned to the observed excited state lifetime at 12 K. The observed lifetime is more than five times longer than the 101 μs gas phase lifetime for the $z\,^8P_{7/2} \rightarrow a\,^6S_{5/2}$ transition and much shorter than the theoretically calculated 3.4 s lifetime for the $a\,^6D_{9/2}$ metastable state of atomic manganese. Decay profiles recorded at higher temperatures showed greater complexity. This behavior is associated with the increased intensity of the 626.8 nm feature at temperatures above 20 K and coincides with the reduction in the 440 nm emission intensity above 20 K. This indicates that the 626.8 nm emission is fed by the state producing the 440 nm band.

The spectral location and long emission decay time strongly support the assignment of the 626.8 nm emission feature to the $a\,^6D_{9/2}$ state of atomic Mn in solid Kr. The similar behavior of the Mn/Ar 625 nm band listed in Table II, suggests the same assignment. Like the $a\,^4D$ state assignment made for the 440 nm emission, the $a\,^6D$ assignment of the 626.8 nm band implies considerable line shape broadening of this D state in the blue site. It also demonstrates a very pronounced shortening in the $a\,^6D_{9/2}$ state lifetime from the calculated gas phase value.

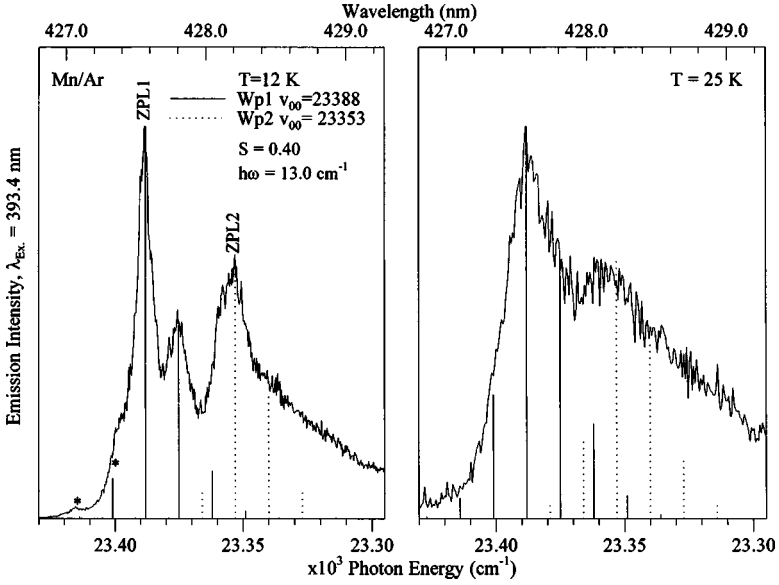

FIG. 7. A comparison of the phonon structure calculated at 12 and 25 K with the W_p function and the resolved emission features recorded in solid Ar with site-specific, pulsed laser excitation at 393.4 nm corresponding to excitation of Mn atoms in the red (1°) site of isolation in Ar. The locations of the zero phonon lines are indicated as ZPL1 and ZPL2 and their values are given by the listed $\nu_{0,0}$ values in wave number units. The presence of hot-phonon emission in the 12 K spectrum is indicated by the two asterisks.

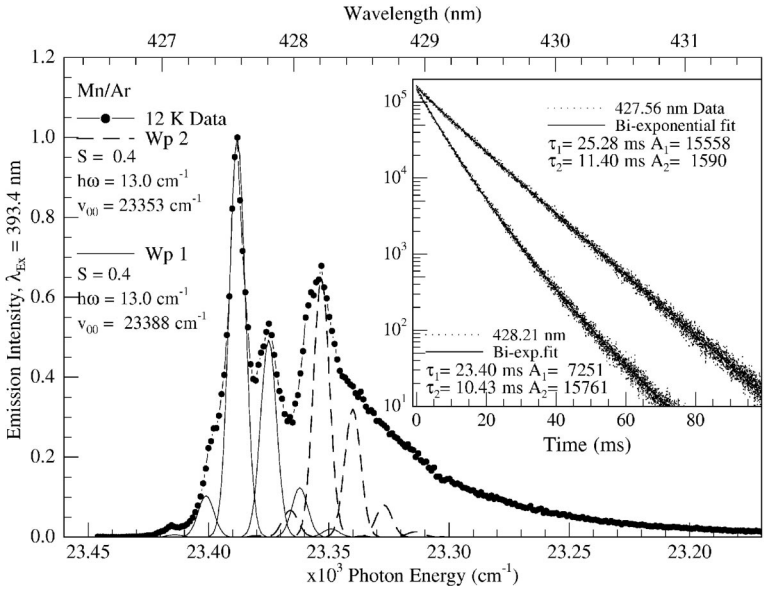

FIG. 8. A comparison of a high-resolution 427.5 nm emission spectrum with the calculated W_p line shapes. The simulation of the emission band profile was generated using Gaussian line shapes (FWHM 6.6 cm^{-1}) for the two identified W_p distributions described in the text. The decay profiles of the 427.56 and 428.21 nm emission bands, shown in the inset, were recorded at 12 K using TCSPC following pulsed laser excitation at 397 nm. This wavelength corresponds to the low-energy threefold split component present on the excitation profile of the red (1°) site.

4. Mn/Ar Red (1°) site: 427.5 nm emission

High-resolution scans of the Mn/Ar 427.5 nm emission recorded at 12 and 25 K and produced with red-site excitation at 393.4 nm are shown on an expanded scale (2 nm range) in Fig. 7. The 12 K spectrum shown on the left, consists of multiple, narrow emission bands, the most intense of which is located at 427.56 nm. Two other resolved features are observed at 427.80 and 428.21 nm. The 427.56 nm feature shows a linewidth of ≈ 6 cm^{-1}, close to the highest resolution achievable with the 0.5 m SP500i monochromator using the 1200 g/mm grating. At higher temperatures, shown for 25 K on the right in Fig. 7, much of the structure is lost due to the considerable broadening exhibited by the emission band. The temperature dependence evident in Fig. 7 was completely reversible with the original spectrum obtained on returning to 12 K. The presence of resolved, narrow lines in the 12 K spectrum and the reversible temperature dependence exhibited, suggests that resolved phonon structure is the origin of the observed emission band shape.

A line shape analysis was conducted on the emission structure using the W_p optical function described in detail by Struck and Fonger[17] and already used by us in our previous Hg/RG work.[19] The contribution of hot phonons (-p terms) to the emission is obtained by multiplying the W_p function, with the appropriate Boltzmann factor. Thus $W_{-p}=[\exp(-p\hbar\omega/kT)]W_p$. As will be shown later, this becomes a significant contribution to the overall emission band shape (even at 12 K) when the phonon frequency is very low. The W_p line shape analysis allows, as shown in our earlier work,[19] identification of the band origin, $v_{0,0}$ i.e., the zero phonon line (ZPL) and an assessment of the electron-phonon coupling strength S (the Huang–Rhys Factor) for the electronic transition involved. The starting point for the W_p line shape analysis is the selection of a value for the phonon frequency ($\hbar\omega$).

To begin the W_p fit, the emission band maximum at 427.56 nm (23 388 cm^{-1}) was chosen as the ZPL. The phonon frequency was selected as 13 cm^{-1} from the splitting between the most intense 427.56 line and the resolved adjacent feature at 427.80 nm. With two of the three adjustable parameters in Eq. (1) of Ref. 19, selected, a fit with the W_p function was conducted by varying the S parameter to generate the recorded intensity distribution. With a very small electron-phonon coupling strength of $S=0.4$, the resulting W_p line shape provides, as shown by the solid vertical lines in the left panel of Fig. 7, a good account of the intense features present in the blue portion of the 12 K spectrum. The fit locates, as indicated by ZPL1, the zero phonon line at 23 388 cm^{-1}. Moreover, it reveals, as indicated by the asterisks in Fig. 7, that the spectral features to higher energy than ZPL1 arise from thermal population in excited phonon levels. The presence of "hot-phonon" emission in the 12 K spectrum might initially seem surprising, however, its origin can be traced back to the low phonon frequency (13 cm^{-1}) extracted in the W_p line shape calculation.

While the W_p line shape analysis achieves good agreement with the high-energy portion of the emission spectrum, not all of the resolved features are accounted for, most notably the band at 428.21 nm. To account for the red features, a second W_p function (W_p2) was included for which $v_{0,0}=23\,353$ cm^{-1} was selected to coincide with the low-energy band at 428.21 nm in the 12 K emission spectrum. A phonon frequency of 13 cm^{-1} was selected, corresponding to the splittings on the main 427.56 nm emission. As shown in Fig. 7, a satisfactory intensity distribution was also achieved with $S=0.4$. The ZPL of the W_p2 function is at 23 353 cm^{-1}, and the intensity distribution, shown by the dotted vertical lines in Fig. 7, accounts for most of the red portion of the emission band profile. With the combined W_p1 and W_p2 functions, all the resolved features present in the emission bands shown in Fig. 7, are accounted for. Simulations generated with the W_p1 and W_p2 functions at $T=25$ K, are compared with the recorded high temperature emission spectrum in the right-hand panel of Fig. 7. The agreement is also good here and demonstrates that the increased bandwidth recorded at 25 K, originates from reduced intensities of the ZPLs and the increased participation of hot-phonon emission, already present even in the 12 K spectrum.

The intensity distributions of the two W_p functions, broadened by a linewidth function, generates the recorded emission band profile quite well. This is evident upon inspection of Fig. 8, where Gaussian curves with a linewidth of 6 cm^{-1}, corresponding to the FWHM of ZPL1, are shown by the solid and dotted traces. It should be noted that the W_p functions do not fully account for the unstructured red wing of the emission. This may indicate the presence of a third, unresolved component that group theory predicts for the excited state responsible for this emission—a possibility treated in the upcoming discussion of the origin of the observed splittings.

Time-resolved measurements indicate, as shown in the inset of Fig. 8, that the decay of the 427.5 nm emission occurs on a very long time scale—0.1 s—clearly revealing the strongly forbidden nature of this transition. A double-exponential function was required to fit of the most intense 427.56 nm emission feature. The fit shown in the inset of Fig. 8, yielded two decay times, 25.28 and 11.40 ms, the longer of which dominates by a factor of 10. The decay curves recorded for the 427.80 nm feature exhibited, although not shown, behavior similar to the dominant 427.56 nm feature. Thus, double-exponential functions were once again required to achieve an adequate fit. The dominant decay component was found at 12 K to have a lifetime of 25.23 ms—the minor had a value of 10.63 ms. The relative amplitudes differed from those observed for the 427.56 nm feature, insofar as the amplitude of the dominant (long) component was only a factor of four times that of the minor (short) component. This indicates the increased importance of the shorter lived component at longer wavelengths.

As shown in Fig. 8, the emission decay profile recorded for the resolved feature at 428.21 nm has a different appearance to that recorded for the 427.56 nm band. The former decay required a double-exponential fit, yielding τ values of 10.43 and 23.4 ms at 12 K but showed a reversal of the amplitudes extracted for the 427.56 nm band. Thus the amplitude of the 10.43 ms component in the 428.21 nm emission, dominates the longer 23.4 ms component by more than a factor of 2. The decay times of the 427.56 and 427.80 nm components are, within the error[25] of the present analysis, equivalent exhibiting dominant matrix lifetimes of 25.28 and 25.23 ms, respectively. The dominant lifetime extracted for the 428.21 nm feature has a value of 10.43 ms.

Identification of the radiative lifetimes is not possible in the present study due to the changes observed in the 427.5 nm emission decay curves with the smallest temperature increase (1.5 K) above the lowest value (12 K) attainable with the displex refrigerator used. It is thereby concluded that the radiative lifetime for the 427.56 nm emission is longer than the 25.3 ms value measured at 12 K. A long decay time of this magnitude requires the assignment of the emission features to a strongly forbidden transition. The location of the emission at 427.56 nm (23 388 cm^{-1}) is consistent with an assignment to the spin and parity "forbidden" $a\,^4D_{7/2} \rightarrow a\,^6S_{5/2}$ transition of atomic manganese which occurs in the gas phase at 23 297 cm^{-1}. Thus, the band at 427.56 nm is blueshifted from the gas phase position by only 92 cm^{-1}, behavior consistent with the narrow emission lines exhibited.

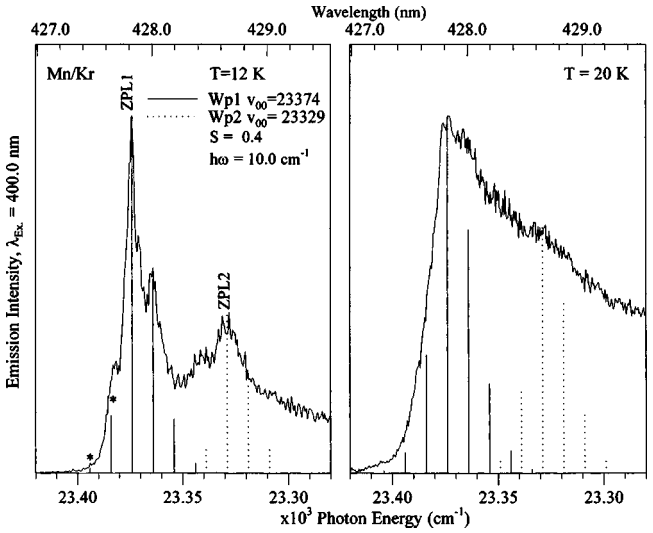

FIG. 9. High-resolution emission spectra recorded at 12 and 20 K with pulsed laser excitation of the red (2°) site in Mn/Kr at 400 nm. Simulations of the resolved emission features were generated with the W_p line shape functions for 12 and 20 K. The location of the zero phonon lines are indicated as ZPL1 and ZPL2, their values are shown by $\nu_{0,0}$ in wave number units.

Successful simulation of the 427.5 nm emission band profile required, as presented in Fig. 8, the use of two sets of W_p function oscillators, exhibiting identical electron-phonon coupling frequencies ($\hbar\omega$=13 cm^{-1}) and strengths (S=0.4) but distinct ZPLs (23 388 and 23 353 cm^{-1}). In light of the W_p line shape analysis, consideration of the recorded emission decay characteristics, summarized in Table II, indicates the longer (25 ms) component corresponds to that of ZPL1 at 427.56 nm while the 10 ms lifetime of the 428.21 nm emission is due to ZPL2. The spectral overlap of these two components, revealed in the W_p1 and W_p2 intensity distributions shown in Fig. 8, is identified as the origin of the double-exponential decay of the lines in the 427.5 nm emission system. Therefore, the requirement of two decay components to achieve adequate fits of the recorded emission decay profiles is attributed to the presence of two distinct electronic transitions. The origin of these transitions in such a small spectral range will be addressed in the Discussion section.

5. Mn/Kr Red (2°) site: 427.8 nm emission

Figure 9 presents high-resolution emission spectra recorded for the 427.8 nm band at 12 and 20 K with laser excitation at 400 nm for a Mn/Kr sample deposited at 12 K and annealed to 38 K. Inspection of the 12 K spectrum, shown in the left panel of Fig. 9, reveals five resolved emission components at 427.68, 427.88, 428.01, 428.40, and 428.65 nm. The spectral location and the narrow linewidth of the emission features are suggestive of a $D \rightarrow S$ type transition. At higher temperatures, the overall emission intensity decreased and the emission broadens as evident in the 20 K spectrum shown on the right in Fig. 9. The narrow 427.8 nm emission bands in Kr parallel in several respects, those ob-

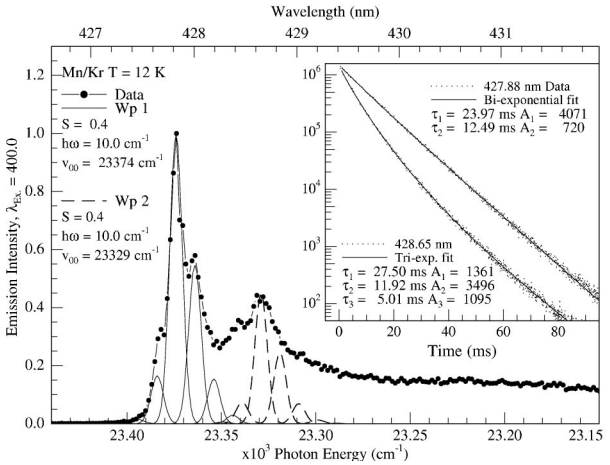

FIG. 10. Simulation of the 427.8 nm emission band profile generated using Gaussian line shapes (FWHM 5.6 cm^{-1}) for both of the W_p distributions as described in the text. The parameters and the positions of the two identified ZPLs ($\nu_{0,0}$) are indicated. Decay profiles of the 427.88 and 428.65 nm emission features recorded at 12 K.

served at 427.5 nm in the Mn/Ar system. This latter emission also resulted from red-site $z\,^6P$ state excitation in solid Ar and was assigned to the $a\,^4D_{7/2} \rightarrow a\,^6S_{5/2}$ transition. The results of a similar W_p line shape analysis conducted on the resolved emission features in the Mn/Kr 427.8 nm system are now summarized.

As was required in the Mn/Ar system, two W_p functions are needed to fit of the observed Mn/Kr bands. The bands located at 427.88 and 428.65 nm were selected as the two ZPLs. Use of the same phonon frequency ($\hbar\omega = 10\ cm^{-1}$) and S value (0.4) allowed, as shown in Fig. 9, an adequate fit of all the resolved features observed at 12 K. The combined W_p functions also provide a good match of the emission linewidth and the intensity distribution observed at 20 K, and accounts well for the asymmetry observed at high energy, as shown in the right panel of Fig. 9. An assessment of the overall quality of the fits is presented in Fig. 10, where Gaussian functions with linewidths of 5.4 cm^{-1}, corresponding to the linewidth of the most intense feature at 23 374 cm^{-1}, are shown.

The decay profile recorded monitoring the most intense resolved emission feature centered at 427.88 nm (corresponding to the ZPL1 in the W_p1 line shape function) at 12 K is presented inset in Fig. 10. An adequate fit of the decay profile was achieved using a double-exponential function that yielded lifetime values of 23.97 ms and 12.49 ms. As indicated by the amplitude values in Fig. 10, the longer decay component (23.97 ms), dominates at 12 K and is thereby identified as the observed lifetime. The same analysis was applied to the emission feature observed at 428.65 nm. This decay profile (shown recorded at 12 K in Fig. 10) exhibited greater complexity, requiring the use of a triple-exponential function to provide an acceptable fit. The dominant decay component had a lifetime of 11.92 ms. This component compares well to the second, short decay component extracted from the analysis of the 427.88 nm feature. The additional third component ($\tau_3 = 5.01$ ms) observed in the decay profile of the 428.65 nm feature, originates from spectral overlap with the 3° site's broad, red-wing emission evident in Fig. 10 beyond 431 nm.

The excited state lifetime identified for the ZPL1 in solid Kr is 24 ms. However, the decay times were observed to be temperature dependent at 12 K, hence the radiative lifetime must be slightly longer than this. A decay time of this magnitude corresponds to a strongly forbidden transition and when the spectral location and emission line shape is considered, the spin and parity forbidden $a\,^4D_{7/2} \rightarrow a\,^6S_{5/2}$ transition at 429.25 nm is the natural assignment for the 427.88 nm emission in Mn/Kr.

6. Red site: 585.8 nm Kr (590 nm Ar) emission

A high-resolution scan of the Mn/Kr 585.8 nm (17 070 cm^{-1}) emission produced with red-(2°) site excitation is shown in the left panel of Fig. 11. The asymmetry of the emission band profile is clearly evident in Fig. 11 as is the narrow "spike" at 17 068 cm^{-1}. Less obvious is an indication of unresolved structure on the blue end of the band. This spike feature is blueshifted from the atomic Mn gas phase $a\,^6D_{9/2} \leftrightarrow a\,^6S_{5/2}$ transition (586.43 nm, 17 052 cm^{-1})

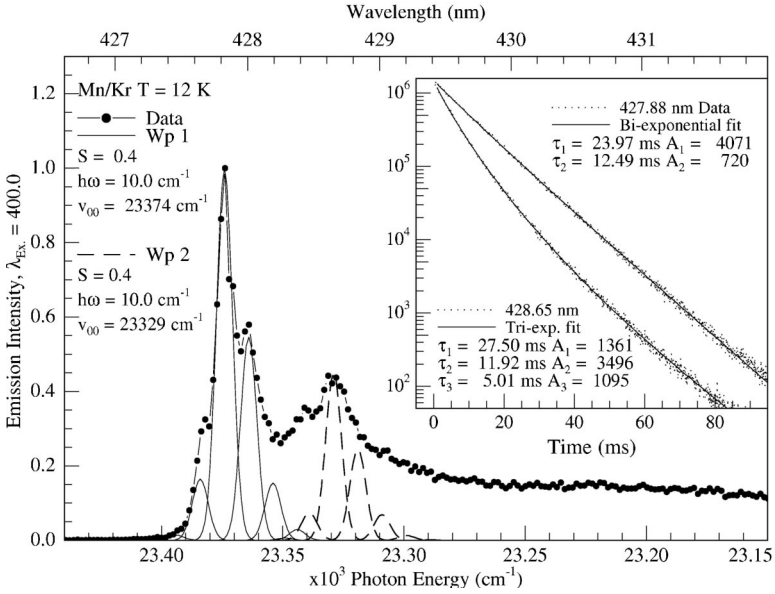

FIG. 11. A High resolution scan of the 585.8 nm emission recorded at 12 K with red-(2°) site excitation of Mn/Kr following annealing to 42 K. A W_p line shape fit is also shown. A decay profile of the 585.9 nm emission recorded at 12 K using TCSPC with pulsed laser excitation at 400 nm is shown on the right.

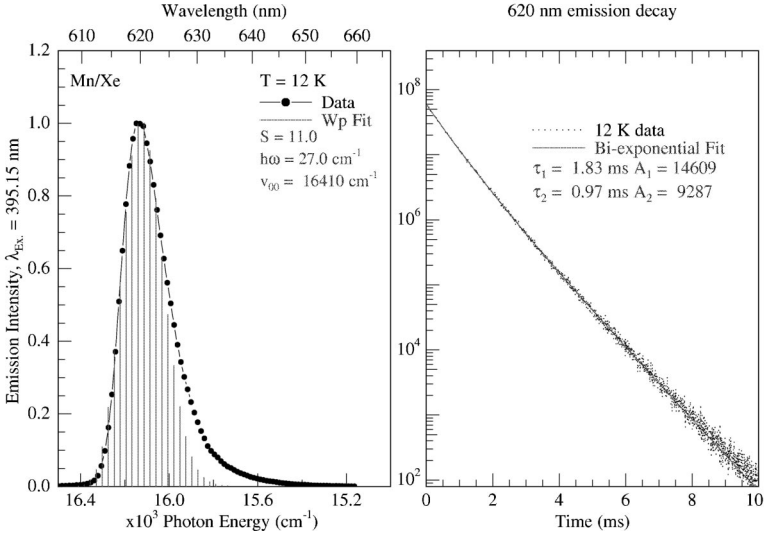

FIG. 12. A time-integrated emission spectrum recorded at 12 K with $z\,^6P \leftarrow a\,^6S$ excitation of Mn/Xe. The W_p line shape was calculated for the 620 nm emission feature at 12 K. The position of the ZPL is indicated by $\nu_{0,0}$ (cm^{-1}). A double-exponential fit of the decay profile recorded for the 620 nm Mn/Xe emission feature is shown in the panel on the right-hand side.

by only 16 cm^{-1}. Recording emission at temperatures in excess of 12 K, resulted in the reduction of the intensity of spike relative to the featureless red wing. The temperature dependence exhibited was completely reversible, an effect characteristic of phonon structure on the emission profile.

The spike and the unresolved structure on the blue end of the 585.8 nm band, prompted the same W_p line shape analysis as conducted on the 427.8 nm band. The W_p1 function shown on the left in Fig. 11 shows quite good agreement with the features on the blue end. Therefore, the ZPL is identified at 585.89 nm (17 068 cm^{-1}) and the unresolved features to the blue of this are hot-phonon emission. Because of the lack of structure on the red wing, fits in this region are not possible. However, two other W_p functions with shifts of 45 cm^{-1} are shown for the purposes of illustrating that the model used to fit the 427.8 nm band can also be used on the 585.8 nm system.

A decay profile recorded at 12 K monitoring the ZPL at 585.89 nm is shown on the right in Fig. 11. Use of a double-exponential fitting function, allowed the extraction of decay components[26] with lifetimes of 287 and 147 μs—the amplitude of the latter dominating by more than a factor of 2. The temperature dependence of the emission decay was not recorded. Thus, with the data presently available, the dominant decay component τ=287 μs is identified as the observed lifetime for the 585.8 nm emission. This value is substantially shorter than the lifetime of 3.4 s calculated for the gas phase $a\,^6D_{9/2} \leftrightarrow a\,^6S_{5/2}$ transition of atomic manganese. However, based on its spectral location and the temperature dependence exhibited, the 585.89 nm emission band is assigned to the ZPL of the $a\,^6D_{9/2} \rightarrow a\,^6S_{5/2}$ transition of atomic Mn in solid Kr. The assignment of this emission feature is discussed in greater depth in a companion paper,[13] in which the 585.8 nm band produced with direct dye laser excitation of the forbidden $a\,^6D \leftarrow a\,^6S$ transition, is recorded and analyzed.

The complex decay characteristics of the Mn/Ar 590 nm emission band, produced with $z\,^6P$ excitation, do not allow a definitive assignment of the $a\,^6D_{9/2} \rightarrow a\,^6S_{5/2}$ transition that has a theoretically predicted[27] gas phase lifetime of 3.4 s. The measured matrix lifetime of 654 μs represents a dramatic shortening of the decay time of the metastable $a\,^6D$ state. However, the spectral position, the asymmetry of the observed emission band and the relatively weak electron-phonon coupling (S=3.3), provide compelling evidence for the assignment of the 590 nm emission to the $a\,^6D$ state. This is further supported by the very similar $\nu_{0,0}$ values of 17 020 and 17 068 cm^{-1} identified in the W_p lineshape fits of the 590 and 585.8 nm bands in Ar and Kr, respectively. As indicated in Table II, the $a\,^6D_{9/2} \rightarrow a\,^6S_{5/2}$ transition occurs at 17 052 cm^{-1} in the gas phase. It is likely that the shortening in the matrix lifetime is induced in the solid state either by the reduced symmetry of the site occupied by Mn atoms or dynamically by vibronic coupling of the $a\,^6D$ state with low symmetry lattice modes.

C. Mn/Xe: 620 nm emission

The absorption spectra presented for Mn/Xe in Ref. 15, indicated the $z\,^6P \leftarrow a\,^6S$ transition of atomic manganese in xenon occurs from a single thermally stable site of isolation centered at 395.5 nm (25 284 cm^{-1}). Figure 12 presents an emission spectrum resulting from lamp excitation at 395 nm, following Mn/Xe sample deposition at 12 K and annealing to 35 K. Inspection of the emission spectrum shown on the left-hand side of Fig. 12 reveals only a single emission feature at 620 nm. The bottom trace on the left in Fig. 13, shows the excitation spectrum recorded for the 620 nm emission. The excitation spectrum shows a well resolved threefold split band, whose components are centered at 392.2, 395.5, and 399.2 nm. The threefold pattern indicates the isolation of Mn atoms within high symmetry sites in solid Xe. Gaussian line shape analysis reveals an average linewidth (FWHM) of $\approx$270 cm^{-1} for each component. As listed in Table I, the band center in Xe is blueshifted from the position of the gas phase $z\,^6P_{5/2} \leftrightarrow a\,^6S_{5/2}$ transition by 496 cm^{-1} (Fig. 13).

To aid the assignment of the emission, a W_p line shape analysis was conducted on the 620 nm band as shown in Fig. 12. Line shapes were generated at 12 K with $\hbar\omega$=27 cm^{-1} using various S values until an adequate fit of the high-energy side of the asymmetric 620 nm emission profile was achieved. The W_p line shape generated at 12 K with $\nu_{0,0}$

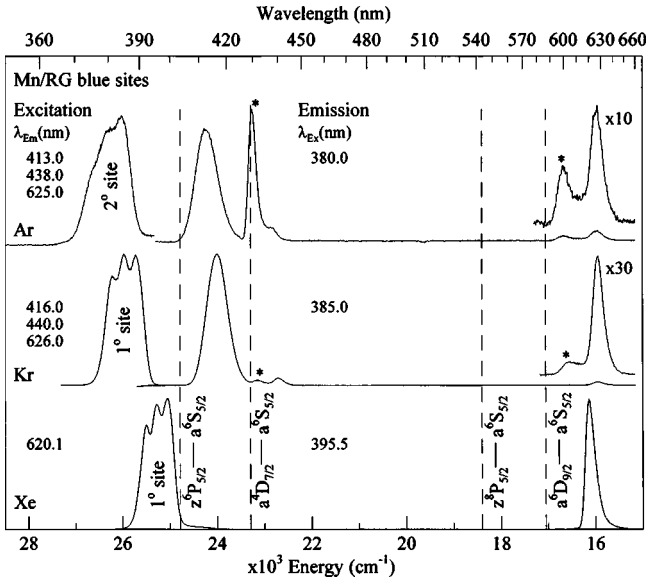

FIG. 13. Emission spectra recorded at 12 K for the Mn/Ar, Mn/Kr, and Mn/Xe systems with site-selective $z\,^6P \leftarrow a\,^6S$ excitation of Mn atoms isolated in the high-energy blue site. The excitation wavelengths used are indicated in the center as λ_{Ex}(nm). The excitation spectra, shown on the left, were recorded by monitoring emission bands as indicated by $\lambda_{Em.}$ in wavelength units. All the spectra shown were recorded following Mn/RG sample annealing. The spectral positions of the gas phase transitions of atomic Mn are shown by the dashed vertical lines. Asterisks indicate remnants of the thermally unstable 3 site of atomic isolation.

$=16\,410\ \mathrm{cm}^{-1}$ (609.38 nm), $\hbar\omega=27\ \mathrm{cm}^{-1}$, and $S=11$ compares well to the observed 12 K emission spectrum, shown on the left in Fig. 12. From the medium S value used, the W_p fit shown in Fig. 12 reveals that the electronic transition producing the 620 nm feature is only moderately coupled to the lattice phonon modes. The band origin ($\nu_{0,0}$) is predicted to occur at $16\,410\ \mathrm{cm}^{-1}$ strongly favoring assignment of the emission to the metastable $a\,^6D$ excited state.

Decay curves of the 620 nm emission feature were recorded using TCSPC following pulsed laser excitation at 395.15 nm corresponding to the central component of the threefold split matrix $z\,^6P \leftarrow a\,^6S$ absorption band. The right-hand panel of Fig. 12 presents the decay profile recorded at 12 K on a semilog plot, following sample annealing to 62 K. A double-exponential fit was required to reproduce the decay profile. The fit shown on the right in Fig. 12, allowed the extraction of two decay times 1.83 ms and 0.97 ms both with substantial amplitudes.

Decay curves of the 620 nm emission feature were recorded at temperatures in excess of 12 K in an attempt to identify the radiative lifetime of the excited state involved in the transition. Both decay components were temperature dependent in the range 12–54 K. The longer ms component identified at 12 K, dominated the decay times extracted at all temperatures up to 54 K where values of 0.85 and 0.23 ms were obtained. As the longer-lived component dominated at all temperatures, this is identified as the observed lifetime τ_{obs}. The decreasing emission intensity and shortening decay time τ_{obs} with increasing temperature for the 620 nm band is attributed to the presence a nonradiative process competing with the emitting level. This nonradiative step is active even in the temperature range 12–16 K. Therefore, the true radiative lifetime of the excited state is longer than the 1.83 ms value measured at 12 K.

The long (1.83 ms) lifetime extracted at 12 K indicates that the 620 nm emission corresponds to a forbidden transition. The gas phase radiative lifetimes τ_{Rad} for the $z\,^8P_{7/2}$ state[24] and metastable $a\,^6D_{9/2}$ states[27] are reported as 101 μs and 3.4 s, respectively. Although the decay characteristics of the 620 nm feature are double exponential, the millisecond lifetimes recorded represent a substantial shortening of the theoretically calculated 3 s gas phase lifetime of the $a\,^6D$ state. More definitively, this lifetime being ten times longer than the $z\,^8P$ state, indicates the $z\,^8P_{5/2} \rightarrow a\,^6S_{5/2}$ transition is not responsible for the 620 nm emission. Based on the present results, the 620 nm emission is tentatively assigned to $a\,^6D_{9/2}$ state, the photophysical characteristics of which are collected in Table II. This assignment is confirmed with direct population of the $a\,^6D$ state with laser excitation, the results of which are presented in Ref. 13.

IV. DISCUSSION

The luminescence resulting from excitation of the $z\,^6P \leftarrow a\,^6S$ transition of atomic Mn isolated in solid Ar and Kr is extremely rich spectroscopically. This originates in part from the number of electronic states lower in energy than the $z\,^6P$ state accessed in photoexcitation and also from the presence in the excitation spectra of two thermally stable sites of atomic isolation. By contrast, the emission in Mn/Xe is quite sparse exhibiting only a single band at 620 nm. This arises because of the single thermally stable site occupied by Mn atoms in Xe samples and very efficient interstate relaxation processes that lead to population of the metastable $a\,^6D$ state.

The differences between the emission spectroscopies recorded for the blue and red sites in annealed Mn/Ar samples are highlighted in Fig. 2. A summary of the data recorded in the corresponding two thermally stable sites in annealed solid Kr is presented in Fig. 3. The positions of the gas phase transitions of atomic Mn are indicated by the vertical lines and the emission features produced by excitation of the thermally unstable 3° site are indicated by the asterisks. Table II presents a summary of the photophysical characteristics of the observed matrix atomic emission, while gas phase data is also included for the purpose of comparison. Consideration of the state-assigned Mn/Ar and Mn/Kr matrix emission reveals that the site of isolation has a profound influence on the relaxation of the $z\,^6P$ excited state of atomic Mn.

A. Red-site emission Mn/Ar and Mn/Kr

Excitation of the red sites produces the 427.5 (and Kr 427.8) nm emission features assigned to the $a\,^6D_{7/2} \rightarrow a\,^6S_{5/2}$ transition and the 590 (585.7) nm emission, assigned to the $a\,^6D_{9/2} \rightarrow a\,^6S_{5/2}$ transition. However, no resonance fluorescence corresponding to the $z\,^6P \rightarrow a\,^6S$ transition is observed with $z\,^6P$ excitation of Mn atoms when isolated in the red sites. The complete absence of the fluorescence indicates an extremely efficient $z\,^6P \Rightarrow a\,^4D$ state relaxation. This intersystem crossing (ISC) competes with 100% efficiency with the nanosecond radiative decay of the

$z\,^6P$ state. The efficiency of this relaxation may originate from a crossing of these two states due to the freedom of the excited $z\,^6P$ state Mn atom to move greater distances in the spatially larger, red site of isolation. This characteristic of the red sites has been discussed in an earlier paper[15] where the site occupancy was identified as tetravacancy, and in which greater spatial freedom exists.

The origin of two ZPLs in the 427.5 (and Kr 427.8) nm emission and their distinct decay times is not immediately obvious. Possible explanations for the pair of ZPLs are now proposed and the deficiencies/merits of each are discussed. The observation of two sets of bands could result from atoms isolated in different sites, in which case, the W_p fits would reflect the interaction of the excited state Mn atom and the sites of isolation. However, it will be remembered that the 427.5 (and Kr 427.8) nm emission system is only produced with selective excitation of the red site. As a result, the emission is that of a single site, thereby ruling out the sites explanation for the pair of ZPLs. The assignment of the resolved emission features to transitions from several of the spin-orbit levels of the $a\,^4D$ excited state of atomic manganese can also be ruled out, given that the spin-orbit interval splittings are much larger in the gas phase than the observed shifts between the ZPLs. Thus, splittings of 252.53, 170.32, and 99.35 cm^{-1} exist between the 7/2, 5/2, 3/2, and 1/2 levels, respectively, values much larger than the 35 cm^{-1} splitting between the two ZPLs identified on the 427.5 nm band in Ar and the 45 cm^{-1} splitting identified in Kr.

It is noteworthy that the decay times recorded for the 427.56 and 428.21 nm emission lines in Ar at 12 K are different, 25 and 11 ms, respectively, indicating that distinct electronic transitions are responsible for the observed features. The corresponding values in Kr are 24 and 12.5 ms. As concluded from the spectral shifts, the 427.5 (427.8 Kr) nm emission has been assigned to the spin and parity forbidden $a\,^4D_{7/2} \rightarrow a\,^6S_{5/2}$ transition. The lifetime has not yet been measured for this transition in the gas phase but calculations[28] indicate a value of thousands of seconds. The final possibility to explain the pair of ZPLs involves crystal field splitting (CFS) of the $J=7/2$ level of the $a\,^4D$ state by the site of isolation. This effect may be manifested by the Mn atom in a "D" state when isolated in a site of either octahedral or tetrahedral symmetry. Thus, the identified energy difference between the two ZPLs (35 cm^{-1}) represents a small crystal field splitting induced in the 7/2 level by the surrounding atomic Ar "ligands." A double group representation of the $J=7/2$ level in an octahedral crystal field, indicates the existence of three distinct electronic levels, two of which are doubly degenerate ($E_{1/2g}$ and $E_{3/2g}$) and one ($G_{3/2g}$) with a fourfold degeneracy. The different degeneracies may be manifested in the distinct decay times observed, i.e., 25 and 11 ms. The CFS explanation may point to the existence of a third CF component in the red wing of the 427.5 nm band. As stated earlier, splittings also exist in tetrahedral symmetry of the tetravacancy site identified as being responsible for the red features in the absorption/excitation spectra. However, the center of inversion designations on the states listed above for octahedral symmetry are then absent. It is likely that the CF splitting on the blue-site $a\,^4D$ state emission at 438 nm is washed out in the stronger electron-phonon coupling (larger S values) exhibited by the Mn atom this site.

A more detailed study is required to ascertain the full crystal field parameters. In this regard, spectroscopy of the 427.8 nm emission band in Ar at temperatures lower than 12 K would be expected to remove the hot-phonon emission thereby resolving more phonon structure and identifying the third CF component. Emission of atomic manganese in neon would also be insightful as the tetravacancy (red) site occupancy would be favored in this host. The higher phonon frequencies in the lighter neon host would also improve resolution of the phonon structure. However, since the same splitting pattern has been identified on the corresponding 427.8 nm band in Mn/Kr, the crystal field interpretation presented here for the $^4D_{7/2}$ state of Mn atoms in the red site of Ar is already strongly supported.

B. Blue-site emission in Mn/Ar, Mn/Kr, and Mn/Xe

Excitation of the $z\,^6P \leftarrow a\,^6S$ resonance transition of atomic Mn isolated in the single thermally stable site in solid Xe results in only one emission feature at 620 nm. High-resolution excitation spectra recorded in the vicinity of the gas phase transition by monitoring the 620 nm band reproduce, as shown in Fig. 13, the threefold split pattern evident in the absorption spectra reported in Ref. 15.

The reported luminescence data strongly favor the assignment of 620 nm feature to emission from the metastable $a\,^6D_{9/2}$ excited state. As the 620 nm band is the only feature observed in the emission spectrum in xenon, the $a\,^6D_{9/2}$ excited state is populated via a 100% efficient relaxation process from the $z\,^6P_{5/2}$ state accessed in excitation. The W_p line shape analysis allowed identification of the electron-phonon coupling strengths for the electronic transition as $S=11$ which is higher than expected for a $D \rightarrow S$ type transition, but comparable in magnitude to the values observed for the blue-site emissions at 625 and 626.8 nm in Ar and Kr, respectively. Although, identification of the radiative lifetime of the observed emission was not possible at 12 K—the lowest temperature attainable in our experiment—an observed lifetime of 1.83 ms was extracted at 12 K. This lifetime represents a shortening by more than three orders of magnitude of the 3 s lifetime reported[24,27] for the gas phase $a\,^6D_{9/2} \rightarrow a\,^6S_{5/2}$ transition of atomic Mn.

C. Red-site/Blue-site luminescence

The lower panels in Figs. 2 and 3, present the emission features produced with $z\,^6P$ state excitation of Mn atoms isolated in the blue sites in Ar and Kr matrices. Table II presents the photophysical characteristics and excited state assignments of the emission features made in the previous sections. The dramatic differences in the emission resulting from blue- and red-site excitation is evident by comparing the band profiles of the observed emission features presented in Fig. 2. As the lower panel shows, blue-site excitation in Ar produces emission features centered at 413, 438, and 625 nm, all of which show broader linewidths than the red-site emission. Excitation of Mn atoms in the blue site of isolation in Kr produces, as shown in the bottom of Fig. 3,

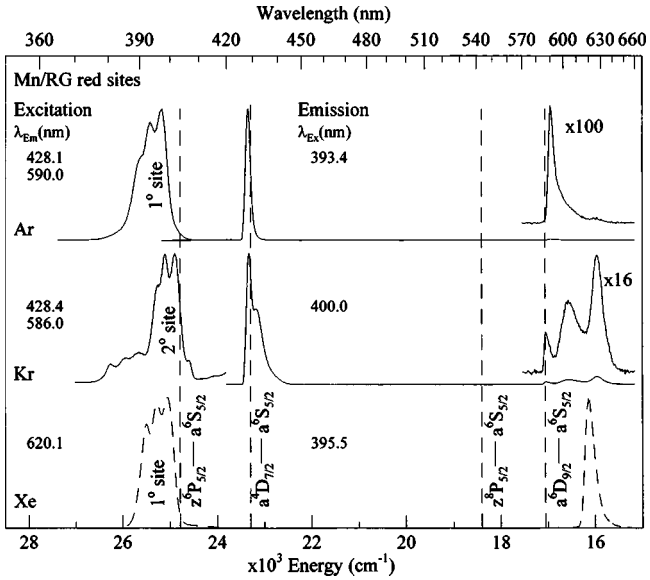

FIG. 14. Emission spectra recorded at 12 K for the atomic Mn/Ar and Mn/Kr systems with red-site excitation. The single thermally stable (blue) site in solid Xe is shown for comparison by the dashed trace.

broad emission at 416, 440, and 626.8 nm. These line shapes are indicative of strong electron-phonon coupling between the guest Mn atom and the blue site in which it resides.

The narrow linewidth emission features produced in Ar and Kr at 427.5 and 427.8 nm, respectively, with red-site excitation are, as shown in Fig. 14, assigned to the $a\,^4D_{7/2} \rightarrow a\,^6S_{5/2}$ transition occurring with 100% efficiency via $z\,^6P \Rightarrow a\,^4D$ intersystem crossing. W_p line shape analyses conducted on these emission features allowed the identification of two ZPLs for the $a\,^4D_{7/2} \rightarrow a\,^6S_{5/2}$ transition in each system. The splitting between the ZPLs was identified as 35 and 45 cm^{-1} in Ar and Kr, respectively. The decay times of the ^4D states in Ar and Kr, while not the radiative lifetimes, are very similar having values of 25 and 24 ms, respectively. The second ZPL had a lifetime of about half this value in Ar and Kr.

Low-energy emission bands centered at 590 and 585.7 nm in Ar and Kr were assigned to the $a\,^6D_{9/2} \rightarrow a\,^6S_{5/2}$ transition of atomic Mn. The lifetimes of these transitions (654 and 287 μs) are considerably shorter than the calculated gas phase value of 3 s. This points to a large (four orders of magnitude) enhancement of the $a\,^6D \rightarrow a\,^6S$ electronic transition in the solid. Consequently, this behavior signals that the metastable $a\,^6D$ state can be pumped relatively easily with laser excitation from the ground state. This excitation was inadvertently done in the Moskovits' earlier LIF work[12] on Mn/Kr, but the resulting emission was attributed to Mn_2. The proposed excitation is demonstrated in a forthcoming publication[13] where tuneable dye laser radiation has been used to record excitation spectra for the electric-quadrupole $a\,^6D_J \leftrightarrow a\,^6S_{5/2}$ ($J=9/2,7/2,5/2,3/2$, and $1/2$) transitions[29] of atomic manganese isolated in the solid rare gases Ar, Kr, and Xe.

Excitation of the blue site produces, as shown in Fig. 13, emission features assigned to $z\,^6P$ state fluorescence at 413 and 416 nm for Mn/Ar and Mn/Kr, respectively, exhibiting similar Stokes' shifts of 2106 and 1936 cm^{-1} and linewidths of 465 and 505 cm^{-1}. The radiative lifetimes of 57.5 and 55.3 ns were extracted for the $z\,^6P \rightarrow a\,^6S$ transitions in solid Ar and Kr. In contrast, Mn/Xe exhibits no resonance $z\,^6P$ fluorescence at all in this site. This behavior indicates that nonradiative relaxation of the $z\,^6P$ state in Xe occurs on a time scale considerably shorter than the nanosecond fluorescence decay times observed in Ar and Kr.

The two emission features located at 438 and 440 nm produced with the blue-site excitation of Ar and Kr matrices have been tentatively assigned to $a\,^4D \rightarrow a\,^6S$ electronic transitions of atomic Mn. These features exhibit similar photophysical characteristics, with linewidths of 230 and 280 cm^{-1} in Ar and Kr, respectively. In addition, these bands share many of the characteristics of the emission features at 625 and 626.8 nm in Ar and Kr. These red emission features in Ar and Kr are tentatively assigned to the a^6D excited state. Examination of the ^6D decay curves in Ar and Kr revealed kinetics consistent with feeding via an ISC mechanism from the $a\,^4D$ state. In solid Xe, the single thermally stable emission feature at 620 nm is assigned to the $a\,^6D_{9/2} \rightarrow a\,^6S_{5/2}$ transition. The three emission bands at 625, 626.8, and 620 nm in the blue site of isolation in Ar, Kr, and Xe are very similar both in their linewidths and spectral positions. The bands are, however, produced in very different amounts with $z\,^6P$ excitation. This is due to more efficient curve crossing processes occurring within the blue site which is thought to correspond to substitutional site occupancy. The topic of site occupancy has been discussed in an earlier contribution[15] in which the blue sites were attributed to single vacancy occupancy. The blue shift on the 620 nm transition in Xe relative to the bands in Ar and Kr, may be a reflection of the more attractive ground state interaction, possible in xenon's larger single substitutional site of isolation.

V. CONCLUSIONS

The excitation spectroscopy recorded for the excited $z\,^6P$ state of atomic Mn isolated in solid Ar, Kr, and Xe allowed the identification of two thermally stable sites in Ar and Kr and a single site in solid Xe. This data allowed the deconvolution of the complicated absorption spectra reported in an earlier contribution into separate site components. The emission spectroscopy reported here revealed two very site-specific relaxation channels in the Mn/Ar and Mn/Kr matrix systems following photoexcitation of the $z\,^6P$ level. Thus, the blue site favors $z\,^6P \rightarrow a\,^6S$ fluorescence while the red site favors $a\,^4D \rightarrow a\,^6S$ phosphorescence. Excited state lifetime measurements definitively assigned $z\,^6P \rightarrow a\,^6S$ fluorescence at 413 and 416 nm in the blue site of Ar and Kr, respectively. Lifetimes of 25 and 24 ms are reported for the first time for the forbidden $a\,^4D_{7/2} \rightarrow a\,^6S_{5/2}$ transition of atomic manganese isolated in the red site in Ar and Kr matrices. Currently, no experimental gas phase lifetime data are available for this transition, which is electric-dipole, magnetic-dipole, and electric-quadrupole forbidden in a one-photon transition.[29]

The W_p line shape analyses of the emission features on the $a\,^4D_{7/2} \rightarrow a\,^6S_{5/2}$ transition in Ar and Kr matrices allowed

the identification of two zero phonon lines and hot-phonon emission with significant intensity—even at 12 K. The occurrence of two distinct zero phonon lines indicates the existence of crystal field splitting for the $a\,^4D_{7/2}$ state of Mn atoms isolated in the red sites in Ar and Kr. The difference between the ZPLs in Ar and Kr is 35 and 45 cm^{-1}, respectively, reflecting the larger crystal field splitting induced by the more polarizable Kr host. In solid Xe, no emission features were assigned to either the $z\,^6P \rightarrow a\,^6S$ or the $a\,^4D \rightarrow a\,^6S$ transitions of atomic Mn. The only band observed in xenon is the metastable $a\,^6D$ state at 620 nm. Mn/Ar and Mn/Kr both produce broad, long-lived emissions in the 625 nm region with blue-site $z\,^6P$ excitation. Like the 620 nm band in xenon, these bands are assigned to $a\,^6D \rightarrow a\,^6S$ transitions, broadened and shifted from the position in the gas phase. These bands were observed in earlier work on Mn/Kr matrices but were assigned to Mn_2. The spectroscopy reported in the previous sections highlights the strong influence the site of isolation has in determining the form of the observed emission bands and the relaxation processes of the excited state guest metal atom, leading to their production.

ACKNOWLEDGMENTS

This research was funded by the Irish Government *Enterprise Ireland*, Basic Science research grant (Grant No. SC/98/403) to whom M.C. gratefully acknowledges receipt of a Ph.D. studentship. The iCCD camera used in this work was acquired with the financial support of Science Foundation Ireland (SFI), Investigator Grant No. 02/IN.1/B032.

[1]D. M. Gruen, in *Cryochemistry*, Spectroscopic Identification and Characterization of Matrix Isolated Atoms, edited by M. Moskovits and G. A. Ozin (Wiley-Interscience, New York, 1976), Chap. 10.
[2]J. C. Rivoal, J. Shakhsemampour, K. K. Zeringue, and M. Vala, Chem. Phys. Lett. **92**, 313 (1982).
[3]C. Crepin-Gilbert and A. Tramer, Int. Rev. Phys. Chem. **18**, 485 (1999).
[4]T. A. Cellucci and E. R. Nixon, J. Phys. Chem. **89**, 1991 (1985), and references cited therein to earlier work, in particular M. T. McKenzie, Ph.D. thesis, University of Pennsylvania, 1983.
[5]M. J. Pellin, D. M. Gruen, T. Fischer, and T. Foosneas, J. Chem. Phys. **79**, 5871 (1983).
[6]H. O. Wiggenhauser, W. Schroeder, and D. M. Kolb, J. Chem. Phys. **88**, 3434 (1988).
[7]S. A. Mitchell, J. Farrell, G. A. Kenney-Wallace, and G. A. Ozin, J. Am. Chem. Soc. **102**, 7702 (1980).
[8]V. A. Braken, P. Gürtler, and J. G. McCaffrey, J. Chem. Phys. **107**, 5290 (1997).
[9]B. Healy and J. G. McCaffrey, J. Chem. Phys. **110**, 3903 (1999).
[10]M. A. Collier and J. G. McCaffrey, J. Chem. Phys. **119**, 11878 (2003).
[11]J. Shakhsemampour, Ph.D. thesis, University of Florida, 1983.
[12]A. D. Kirkwood, K. D. Bier, J. K. Thompson, T. L. Haslett, A. S. Huber, and M. Moskovits, J. Phys. Chem. **95**, 2644 (1991).
[13]M. A. Collier and J. G. McCaffrey, J. Chem. Phys. (submitted).
[14]M. A. Collier, Ph.D. thesis, National University of Ireland Maynooth, 2004, document available on-line at http://eprints.may.ie/archive/00000154/01/MartinCollierThesis.pdf
[15]M. A. Collier and J. G. McCaffrey, J. Chem. Phys. **122**, 054503 (2005).
[16]NIST Atomic Spectra Database, website: http://physics.nist.gov/cgi-bin/AtData/ (last accessed 4 February 2004).
[17]C. W. Struck and W. H. Fonger, *Understanding Luminescence Spectra and Efficiency Using Wp and Related Functions* (Springer, Berlin, 1991).
[18]V. A. Bracken, P. Gürtler, and J. G. McCaffrey, J. Chem. Phys. **107**, 5290 (1997).
[19]M. A. Collier and J. G. McCaffrey, J. Chem. Phys. **119**, 11878 (2003).
[20]D. V. O'Connor and D. Philips, *Time-correlated Single Photon Counting* (Academic, London, 1984).
[21]The relative intensities of the 427.5 nm and 590 nm emission features produced with site-selective excitation at 393.4 nm of the (1° site) in Mn/Ar can be extracted from the emission spectrum shown, as the resolution used was constant throughout the scan.
[22]S. S. Cohen and M. L. Klein, in *Inert Gases—Potentials, Dynamics and Energy Transfer in Doped Crystals*, Dynamics of Impure Rare-Gas Crystals, edited by M. L. Klein (Springer, Berlin, 1984), Chap. III.
[23]The index of refraction used for solid Kr at 241 nm is 1.428 at 12 K [P. Gürtler (unpublished)].
[24]S. M. Younger, J. R. Fuhr, G. A. Martin, and W. L. Wiese, J. Phys. Chem. Ref. Data **7**, 495 (1978).
[25]The error on the lifetimes extracted from emission decay curves recorded with the multichannel scaler and photon counting PMT is in the region of 1% when double-exponential fits are made.
[26]The fit conducted to the decay profile recorded monitoring the 585.8 nm emission feature produced with red-(2°) site excitation at 400 nm is truncated at early time $\approx 40\ \mu s$. This was required due to pulse-pile up in emission.
[27]A. A. Radzig and B. M. Smirnov, *Reference Data on Atoms, Molecules and Ions* (Springer, Berlin, 1985).
[28]G. A. Martin, J. R. Fuhr, and W. L. Wiese, J. Phys. Chem. Ref. Data **17**, 1 (1988).
[29]R. D. Cowan, *The Theory of Atomic Structure and Spectra* (University of California Press, Berkeley, CA, 1981), pp. 445–448.